Low-frequency dynamics of $LiCu_3O_3$: An antiferromagnet on a strongly depleted square lattice

S. K. Gotovko [1,2] A. G. Ivanova [3] P. S. Kudimkina [1,2] A. A. Bush [4] V. I. Kozlov [1,4]
M. Hemmida [5] H.-A. Krug von Nidda [5] and L. E. Svistov [1,*]

[1] *P.L. Kapitza Institute for Physical Problems, RAS, 119334 Moscow, Russia*
[2] *HSE University, 101000 Moscow, Russia*
[3] *Shubnikov Institute of Crystallography, Kurchatov Complex Crystallography and Photonics of NRC "Kurchatov Institute", 119333 Moscow, Russia*
[4] *MIREA - Russian Technological University, pr. Vernadskogo 78, 119454 Moscow, Russia*
[5] *Experimental Physics V, Center for Electronic Correlations and Magnetism, Institute of Physics, University of Augsburg, D-86135 Augsburg, Germany*

(Received 26 November 2024; revised 10 February 2025; accepted 12 February 2025; published 28 February 2025)

We present the study of low-frequency dynamics of $LiCu_3O_3$—an antiferromagnet on a strongly depleted square lattice. The crystal structure contains two types of square planes with different $Li^+ \rightarrow Cu^{2+}$ substitution rates (20% and 40%). Recent nuclear magnetic resonance (NMR), magnetization measurements and neutron scattering experiments revealed the occurrence of antiferromagnetic order at $T_{c1} = 123$ K and the change of the magnetic state at $T_{c2} \approx 30$ K. Electron spin resonance (ESR) intensity measurements confirmed that at $T_{c1} = 123$ K a magnetic phase transition of only a part of the sample occurs, while the rest of the sample remains paramagnetic. Supposedly, the order occurs in the magnetic planes with higher concentrations of magnetic ions. The ratio of ESR intensity values before and after the transition is in agreement with this suggestion. In the studied frequency and temperature range (18–140 GHz, 30–300 K) only one electron paramagnetic resonance (EPR) branch was observed. At temperatures $T < 30$ K, the ESR branch acquires a gap which gradually increases with temperature decrease. The behavior of the observed gap in the magnetic resonance spectra indicates that this gap is, in fact, a pseudogap of exchange nature associated with finite-sized clusters of magnetic ions.

DOI: 10.1103/PhysRevB.111.064430

I. INTRODUCTION

The influence of nonmagnetic substitution of magnetic ions in antiferromagnets on their magnetic properties has been a subject of great interest for a long time. Low-dimensional antiferromagnets are highly sensitive to nonmagnetic dilution. Indeed, the presence of any amount of nonmagnetic impurities in one-dimensional (1D) antiferromagnetic chain makes the occurrence of a long-range order impossible even at $T = 0$. The influence of weak doping on magnetic properties of 1D antiferromagnets with weak interchain interactions (quasi-1D AF) were studied theoretically and experimentally in Refs. [1–7]. The object of the study presented in this work is a quasi-2D antiferromagnet on a diluted square lattice. In the frames of different approaches, the temperature evolution of nearest-neighbor correlations in such magnets with different degree of dilution has been studied in Refs. [8–10]. The best experimental realization was presented in examples of quasi-2D magnets $La_2Cu_{1-x}(Zn,Mg)_xO_4$ [11,12], $Li_2V_{1-x}Ti_xOSiO_4$ [13], and La_2CuO_4 doped with Li and Sr [14]. In $La_2Cu_{1-x}(Zn,Mg)_xO_4$, a high doping rate with Zn and Mg is possible which allows experimental confirmation of the theoretical predictions.

$LiCu_3O_3$ is a novel representative of cuprates with mixed valence with spin $S = 1/2$ on a depleted square lattice. It is a unique example of such systems not only because of the high dilution rate but also because the crystal structure of this compound exhibits two types of square lattices with different dilution ratios simultaneously: $x_A = 0.2$ in one plane and $x_B = 0.4$ in another plane. These features are an inherent characteristic of the $LiCu_3O_3$ crystal structure. The dilution ratio of 0.4 is extremely close to the percolation threshold of a square lattice, $x_p \approx 0.41$, which makes the establishment of the long-range order in separate planes problematic [9,12].

In this work, we discuss the magnetic properties of $LiCu_3O_3$ studied with electron spin resonance (ESR) spectroscopy. The crystallographic lattice of this material consists of stacked alternating square planes -C-B-A-B-C-, where nonmagnetic Cu^+ ions occupy sites of C planes, and nonmagnetic Li^+ and magnetic Cu^{2+} ions are placed in the sites of A and B square planes (Fig. 1). O^{2-} ions from A planes are positioned precisely in the center of the Cu^{2+}-Li^+ squares, whereas oxygen ions from B planes are slightly shifted from the centers towards C planes. Magnetic Cu^{2+} and nonmagnetic Li^+ ions are distributed in A and B planes with fractional occupancies of 0.8:0.2 and 0.6:0.4, respectively. The crystal structure of $LiCu_3O_3$ and Cu^{2+}/Li^+ distribution has been studied with x-ray diffraction and neutron scattering experiments in several works [15–18], the results of which identified the same

*Contact author: svistov@kapitza.ras.ru

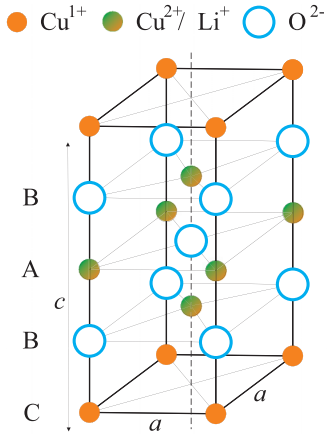

FIG. 1. Crystal structure of $LiCu_3O_3$. The orange circles mark the positions of the Cu^+ nonmagnetic ions, while the orange-green circles in B-A-B square planes mark the positions of randomly distributed ions of nonmagnetic Li^+ and magnetic Cu^{2+}. The larger blue open circles are at the positions of the O^{2-} ions.

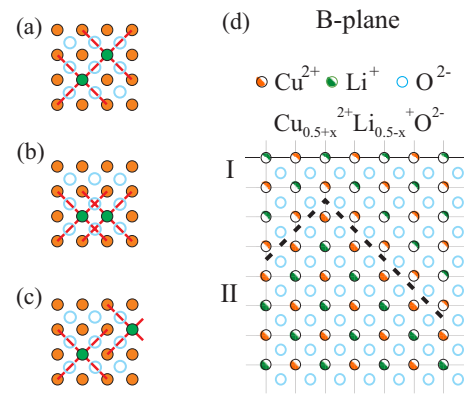

FIG. 2. [(a)–(c)] Schema of possible incrustation of Li^+ ions in CuO matrix. Dashed lines mark d-p-d bonds between Cu^{2+} ions destroyed by Li^+ doping. (d) Domain structure of $LiCu_3O_3$ in B plane. Half-shaded orange and green circles represent Cu^{2+} and Li^+ ions from different domains (I and II). Blue circles are oxygen ions. Black dashed line shows the domain boundary.

crystallographic structure and similar Cu^{2+}/Li^+ ratios for A and B planes. No indications for any superstructure or additional crystallographic phases were observed at the moment, therefore Cu^{2+} and Li^+ ions can be considered as uniformly distributed in A and B planes.

II. CRYSTAL STRUCTURE OF $LiCu_3O_3$

The crystal structure of $LiCu_3O_3$ belongs to the space group $P4/mmm$ at room temperature with lattice parameters $a = 2.810$ Å and $c = 8.889$ Å [15]. The unit cell diagram of the $LiCu_3O_3$ crystal structure is shown in Fig. 1(a). Single crystals of $LiCu_3O_3$ were grown with flux method from high-temperature solutions of Li_2CO_3 and CuO at rapid cooling down from $T = 915$ K to room temperature [19].

It is natural to expect that during the growth process at high-temperature Cu^{2+}/Li^+ ions are distributed randomly. Nevertheless, the diffusive redistribution of Li^+ ions into more energetically favorable positions during the cooling process is also possible. In Ref. [20], it has been shown that it is more energetically favorable for two Li^+ ions to substitute Cu^{2+} ions from nearest diagonal sites as shown in Fig. 2(a) than when it occupies two nearest or isolated sites [Figs. 2(b) and 2(c)]. Such a conclusion was made by the authors as the result of exact diagonalization (ED) and DFT calculations. Qualitatively, this result seems reasonable, because the amount of destroyed covalent d-p-d bonds between Cu^{2+} ions is minimized in such a configuration. As a result, one can expect the formation of "islands" in which Cu^{2+}/Li^+ ions are placed in chessboard order at ratio 0.5:0.5. Note that the realization of such structure is possible in form of two crystallographic domains which differ by the shift by one period along the side of the square lattice. Figure 2(d) shows a fragment of such ordered structure with two domains; boundaries between these domains contain more Cu^{2+} than the inner area of the domains.

In this model, in A planes, $Cu_{0.5}Li_{0.5}O$ "islands" are expected to be integrated in the infinite CuO-matrix. The composition $Cu_{0.6}Li_{0.4}O$ of B planes is close to $Cu_{0.5}Li_{0.5}O$. According to Ref. [20], each B plane is built with small domains of regular $Cu_{0.5}Li_{0.5}O$ arrangement, and the surplus of Cu^{2+} in relation to 0.5:0.5 ratio can be compensated by the formation of a developed domain structure with the characteristic size of domains $l_0 \approx 10a$.

At the moment, there is no valid information about the nanoscale distribution of the Cu^{2+}/Li^+ ions realized in $LiCu_3O_3$. Hence, the experimental results will further be discussed in the frames of both nonstochastic [20] and random Cu^{2+}/Li^+ distribution models [19]. Keep in mind that the most realistic scenario is the superposition of the suggested models.

III. MAGNETIC PROPERTIES

Magnetic properties of $LiCu_3O_3$ were studied in Refs. [18–20] by means of magnetometry, NMR and elastic neutron scattering. As the result of these experiments, it was observed that at $T_{c1} \approx 123$ K antiferromagnetic order occurs.

Neutron scattering experiments revealed that the wave vector of the established antiferromagnetic structure is $\mathbf{k} = (1/2, 0, 1/2)$. Such value of $\mathbf{k}$ indicates that the dominant antiferromagnetic in-plane interaction is between Cu^{2+} ions positioned in diagonal sites of the square lattice. The absolute value of magnetic susceptibility obtained in magnetization measurements allows to give a rough estimation of the dominant antiferromagnetic exchange: $J \approx 100$ K. The anisotropy of magnetic susceptibility and results of elastic neutron scattering experiments revealed the presence of a fourfold anisotropy in the plane perpendicular to the C_4 axis. The axes [100] and [010] are the easy axes for antiferromagnetic vector $\mathbf{l}$. At the same time, the observed anisotropy of susceptibility for magnetic field $\mathbf{H}$ directed along and perpendicular to $\mathbf{l}$ is only about 6%, which is relatively small considering the fact that in case of a classic collinear antiferromagnet one could expect it to be 100%.

^{7}Li NMR studies have shown that at $T < 123$ K local fields on nuclear spins and, thus, the directions of magnetic

moments have a continuous distribution. For NMR spectra, the linewidth can be satisfactorily described when only dipole fields are taken into account and in the assumption that the value of Cu^{2+} magnetic moment is $\approx 0.5\mu_B$. Magnetometry and NMR studies revealed that at $T_{c2} \approx 30$ K the magnetic state of $LiCu_3O_3$ significantly changes. The transition from high-temperature phase to low-temperature phase does not manifest itself as a sharp irregularity. In Refs. [19,20], the high-temperature singularity is attributed to the establishment of a collinear antiferromagnetic order, and the low-temperature singularity is ascribed in Ref. [19] to the change of magnetic state in B planes. In this work, the results of a study of $LiCu_3O_3$ magnetic properties by means of ESR are presented.

IV. CHARACTERIZATION OF SAMPLES AND EXPERIMENTAL TECHNIQUES

In our experiments, we have studied single crystals of $LiCu_3O_3$, which were grown from high-temperature solutions of Li_2CO_3 and CuO in ambient atmosphere [17,19]. The samples were approximately $3 \times 3 \times 0.5$ mm^3 of size with the developed plane perpendicular to the C_4 axis of the crystals. The developed planes of the plate were mirrorlike smooth and had shapes close to a rectangular with the sides directed along [110] and [1$\bar{1}$0] axes of the crystal. The results of the experiments were reproducible and did not vary from sample to sample. The crystals were from different batches including the batch used in the previous NMR and magnetization studies of magnetic properties [19].

One of the crystals with dimensions of $0.16 \times 0.11 \times 0.04$ mm^3 was additionally examined with the Xcalibur EosS2 single crystal x-ray diffractometer. The detailed description of the crystal structure study is given in Appendix. Stoichiometric composition was $Cu_{2.96}Li_{1.06}O_3$. The obtained space group $P4/mmm$ and the lattice parameters $a = 2.81386(2)$ Å, $c = 8.89950(8)$ Å are in agreement with those reported previously, the occupancies of Li^+ partially substituting Cu^{2+} in the positions Cu(2) and Cu(3) forming the A and B planes were 18.5% and 43.5%, respectively, which are close to the 20% and 40% reported in Refs. [15,16].

The EPR (electron paramagnetic resonance) measurements at $\nu = 9.34$ GHz were conducted at a Bruker Elexsys E500A x-band spectrometer equipped by an Oxford helium gas-flow cryostat ESR 900 covering the temperature range 4.2 K $\leqslant T \leqslant$ 300 K. By that cryostat only the sample space is cooled while the rectangular standard cavity, Bruker ER 4102ST, remains at room temperature. Thus, its quality factor $Q \approx 3000$ is practically temperature independent. Due to the lock-in technique with 100 kHz field modulation the field derivative of the power reflected from the sample was recorded dependent on the external magnetic field. The $LiCu_3O_3$ single crystal was fixed with paraffin in a Suprasil quartz-glass tube. A programmable goniometer allowed angular dependent measurements with well defined steps within the *ac* plane.

Multi-frequency measurements were conducted with the use of the ESR setup which was equipped with a multiple mode rectangular resonator of the transmission type. The frequency range was 18 GHz $< \nu <$ 140 GHz and magnetic field was up to 7 T. The sample was glued on a rotating holder which allowed to rotate the sample with respect to the external magnetic field. During the experiment, the temperature was varied between 1.3 and 80 K.

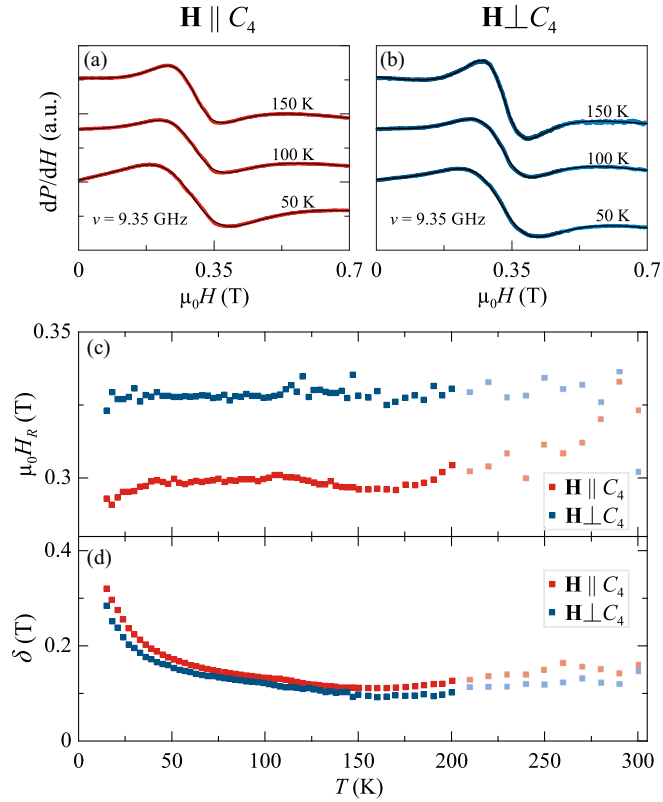

FIG. 3. (a) and (b) examples of spectra measured at $\nu = 9.35$ GHz at two mutually orthogonal orientations of external magnetic field **H**: **H** ∥ C_4 (a) and **H** ⊥ C_4 (**H** ∥ [110]) (b). Black lines present the results of spectra approximation described in text. (c) Temperature dependence of H_R. (d) Temperature dependence of linewidth $\delta(T)$. Red squares correspond to **H** ∥ C_4, blue squares correspond to **H** ⊥ C_4.

V. EXPERIMENTAL RESULTS

A. X-band EPR measurements

Figures 3(a) and 3(b) show the examples of EPR lines measured at two orientations of magnetic field, **H** ∥ C_4 and **H** ⊥ C_4, at different temperatures, $\nu = 9.34$ GHz. The field scans can be successfully approximated with the derivative of a Lorentzian function with a small additional contribution linear in field. The results of this approximation are shown in Figs. 3(a) and 3(b) with black solid lines. Panels (c) and (d) of Fig. 3 present temperature dependences of the parameters of the spectra: resonance field H_R and linewidth δ obtained as the result of lines approximation, respectively. The parameters obtained in these measurements (H_R and δ) were determined with the precision of 5%. The sample temperature was controlled by a helium-gas flow cryostat, thus, the resonator's quality factor and frequency out of the absorption region did not depend on the sample temperature at $T < 200$ K, which allowed simple comparison of integral absorption of EPR lines (I) at different temperatures up to $T \approx 200$ K. At

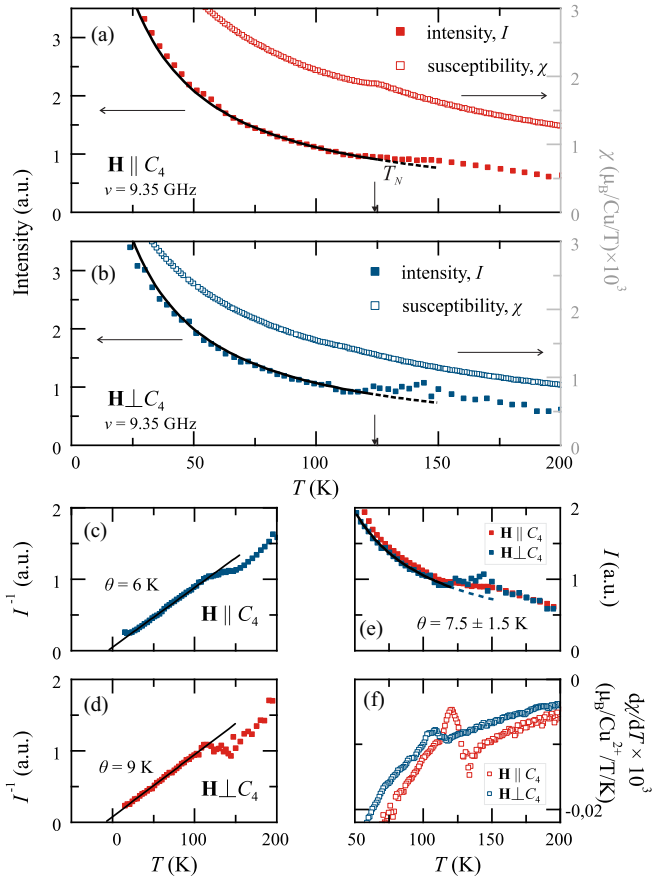

FIG. 4. [(a) and (b)] Temperature dependencies of integral intensity of resonance absorption I (solid squares) and magnetic susceptibility χ (open squares) at $\mu_0 H = 0.3$ T. Axes on the left (black) correspond to intensity data and axes on the right (grey) correspond to magnetization data. Solid lines show approximation of $I(T)$ with the Curie-Weiss law. Dashed lines show extrapolations of $I(T)$ at $T > T_{c1}$. Arrows at abscissa axes show the temperature T_{c1} obtained in Refs. [18,19]. [(c) and (d)] Reverse intensities $I^{-1}(T)$ from (a) and (b). Solid lines show linear approximation of $I^{-1}(T)$ dependences at 30 K $< T <$ 100 K. Dashed lines show the extrapolation of $I^{-1}(T)$ at $T > T_{c1}$. (e) Integral intensity of resonance absorption from (a) and (b) in the vicinity of the peculiarity. Solid line shows Curie-Weiss law dependence with $\theta_A = 7.5$ K, dashed line shows the extrapolation of $I(T)$ at $T > T_{c1}$. (f) Temperature derivative of the magnetic susceptibility $\chi(T)$ in the vicinity of the peculiarity.

$T > 200$ K, the parameters of the resonator change due to the temperature dependent conductivity of $LiCu_3O_3$ at this temperature range.

The value of H_R is almost temperature-independent at 30 K $< T <$ 175 K [Fig. 3(c)]. In the vicinity of the transition into antiferromagnetic state at $T_{c1} = 123$ K no distinct anomalies of EPR linewidth were observed. In contrast, the temperature dependence of the integral absorption line intensity $I(T)$ demonstrates a kink, as shown in Figs. 4(a) and 4(b). The arrows at the abscissa axes show the transition temperature T_{c1} obtained in neutron scattering and NMR experiments [18,19]. Additionally, the temperature dependence of magnetic susceptibility measured at $\mu_0 H = 0.3$ T is presented in Figs. 4(a) and 4(b) with open symbols with ordinate axis on the right. At 30 K $< T < T_{c1}$, the temperature dependence of the integral absorption line intensity can be satisfactorily described by a Curie-Weiss law with the constant $\Theta = 7.5 \pm 1.5$ K as presented in Figs. 4(c) and 4(d). This dependence extrapolated to higher-temperature region $T > T_{c1}$ is shown in Figs. 4(a) and 4(b) with black solid lines. Figures 4(e) and 4(f) illustrate the temperature dependences of $I(T)$ and temperature derivative of $\chi(T)$ in the vicinity of T_{c1}, respectively. It can be seen from Figs. 4(a)–4(d) that below the magnetic ordering temperature, the absorption intensity decreases by approximately 25%. This observation naturally leads to the conclusion that at T_{c1} the number of magnetic ions present in the paramagnetic state decreases. It is natural to expect the resonance frequency of the magnetically ordered part to differ from the EPR frequency, which leads to the decrease of EPR signal intensity. Magnetic division of the sample in magnetically ordered and paramagnetic parts at 30 K $< T < T_{c1}$ was suggested in Ref. [19] as the result of the analysis of magnetization measurements. This scenario suggests that at $T = T_{c1}$ only magnetic ions from the A plane become magnetically ordered while the magnetic ions from strongly depleted B plane remain in paramagnetic state.

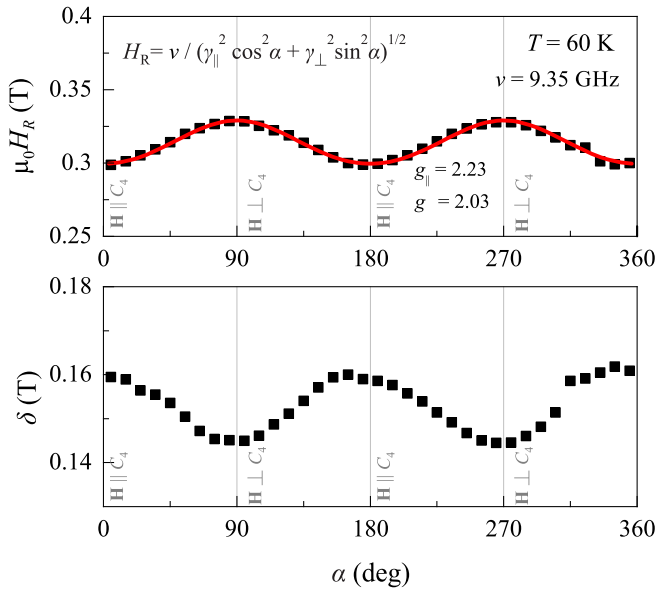

FIG. 5. (Top) Angular dependence of H_R. The magnetic field was rotated from $\mathbf{H} \parallel C_4$ to $\mathbf{H} \perp C_4$ ($\mathbf{H} \parallel [110]$). Solid line shows the approximation of the dependence with the formula shown in the figure. (Bottom) Angular dependence of linewidth δ. $\nu = 9.35$ GHz. α is the angle between $\mathbf{H}$ and C_4 axis.

On decreasing temperature below 30 K, the EPR linewidth δ increases, and the EPR line starts shifting towards lower fields. At $T < 15$ K, no resonance absorption at $\nu = 9.35$ GHz was observed, which indicates that the EPR spectrum acquires a frequency gap.

Angular dependencies of resonance field H_R and EPR linewidth δ measured at $\nu = 9.35$ GHz and $T = 60$ K are presented in Fig. 5. The magnetic field $\mathbf{H}$ was rotated in the $(1\bar{1}0)$ plane of the crystal (from [110] axis to C_4 axis). Anisotropy in (001) plane was not observed. The angular dependencies

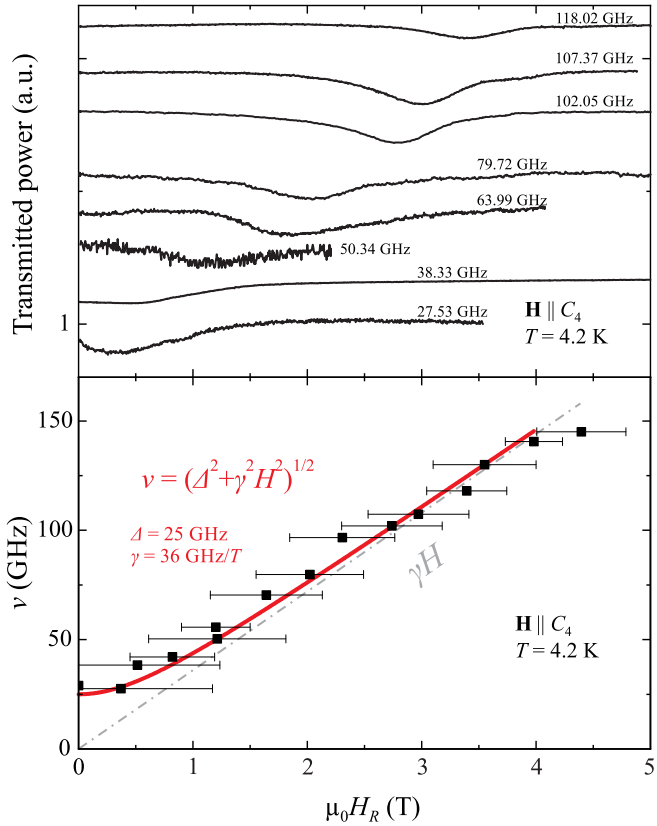

FIG. 6. (Top) Examples of P_{tr} field scans measured at $T = 4.2$ K. The scans were normalized to 1 and stacked along ordinate axis for clarity. (Bottom) The frequency-field diagram measured at $\mathbf{H}\|C_4$, $T = 4.2$ K. The ESR resonances are marked by solid symbols. Segments at each point indicate HWHM of corresponding absorption lines. The red line shows the result of quasilinear approximation with parameters given in text. The dash-dotted line is the paramagnetic $\nu(H)$ with $\gamma = 36$ GHz/T.

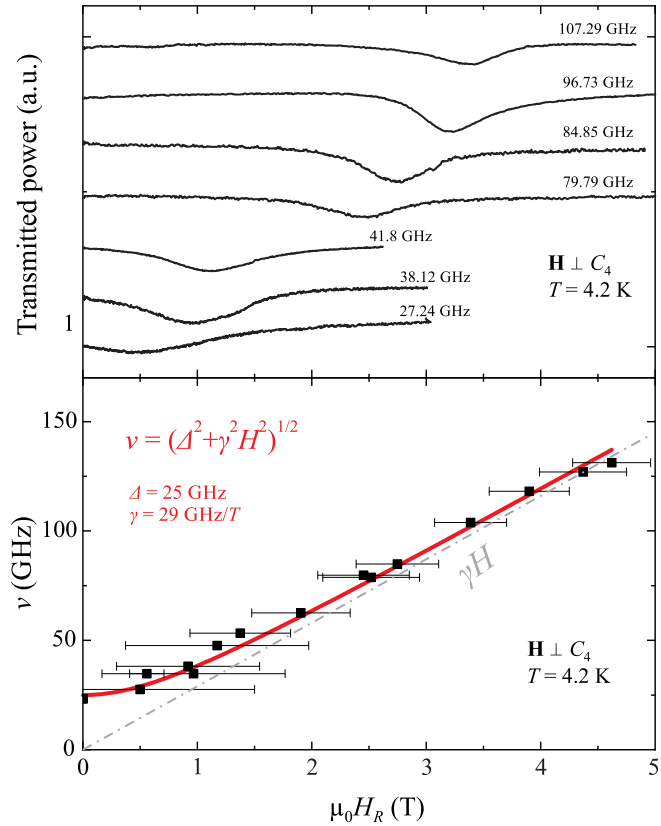

FIG. 7. (Top) Examples of P_{tr} field scans measured at $T = 4.2$ K. The scans were normalized to 1 and stacked along ordinate axis for clarity. (Bottom) The frequency-field diagram measured at $\mathbf{H}\|[110]$, $T = 4.2$ K. The ESR resonances are marked by solid symbols. Segments at each point indicate HWHM of corresponding absorption lines. The red line shows the result of quasilinear approximation with parameters given in text. The dash-dotted line is the paramagnetic $\nu(H)$ with $\gamma = 29$ GHz/T.

of H_R are well explained with the uniaxial anisotropy of the g factor: $g_\parallel = 2.23$, $g_\perp = 2.03$, where indices $\parallel$ and $\perp$ refer to mutual orientation of C_4 axis and external field. The expression describing the angular dependence $H_R(\alpha)$ is shown in the figure. Such anisotropy of g factor is characteristic for Cu^{2+} ions with one electron hole in the $d_{x^2-y^2}$ orbital. The similar situation was observed in cuprates $LiCuVO_4$ and $LiCu_2O_2$. Note that the observed absolute value of the linewidth is also comparable to those two cuprates. We will comment on that point below in the discussion.

B. Multifrequency ESR measurements

The top panels of Figs. 6 and 7 provide examples of the field scans of high-frequency power $P_{tr}(H)$ transmitted through the resonator at $T = 4.2$ K for $\mathbf{H} \parallel C_4$ and $\mathbf{H} \perp C_4$ ($\mathbf{H} \parallel [110]$), respectively. The scans were normalized to 1 in the field range far from resonance peculiarity and stacked along ordinate axes for clarity. The frequency dependences of resonance fields corresponding to the absorption lines from the top panels are shown by solid symbols in the bottom panels of the figures. The segments given at each point illustrate the values of the width at the half-maximum (HWHM) of the corresponding absorption lines. Only one quasilinear branch $\nu(H_R)$ was observed which can be roughly approximated with dependence $\nu = \sqrt{\Delta^2(T) + \gamma^2 H_R^2}$. Here, for $\mathbf{H}$ parallel to C_4 axis $\gamma_\parallel(T = 4.2\ \text{K}) = 36$ GHz/T and for $\mathbf{H}$ perpendicular to C_4 axis $\gamma_\perp(T = 4.2\ \text{K}) = 29$ GHz/T in contrast to $\gamma_\parallel = 31.2$ GHz/T and $\gamma_\perp = 28.4$ GHz/T measured at $T > 30$ K. $\Delta(T > 30K) = 0$, and Δ increases when temperature decreases; $\Delta(T = 4.2\ \text{K}) = 25 \pm 3$ GHz. The $\nu(H)$ dependence asymptotically tends to the paramagnetic gapless resonance $\nu(H) \to \gamma H$ shown by the dash-dotted lines. Excitation of this branch was effective when the magnetic component of UHF-radiation $\mathbf{h}$ was perpendicular to the external magnetic field: $\mathbf{h} \perp \mathbf{H}$.

No additional absorption lines were observed in our experiments at temperatures 1.3 K $< T <$ 80 K, at 18 GHz $< \nu <$ 140 GHz, and magnetic fields 0 T $< \mu_0 H <$ 7 T.

The top panels of Figs. 8 and 9 show the temperature evolution of $P_{tr}(H)$ scans at $\nu = 27.53$ and $\approx$77 GHz, respectively, measured at two different field orientations. The frequency $\nu = 27.53$ GHz is close to the value of the frequency gap at $T = 4.2$ K. The $P_{tr}(H)$ scans were normalized to 1 at fields far from H_R and stacked along the ordinate axis for

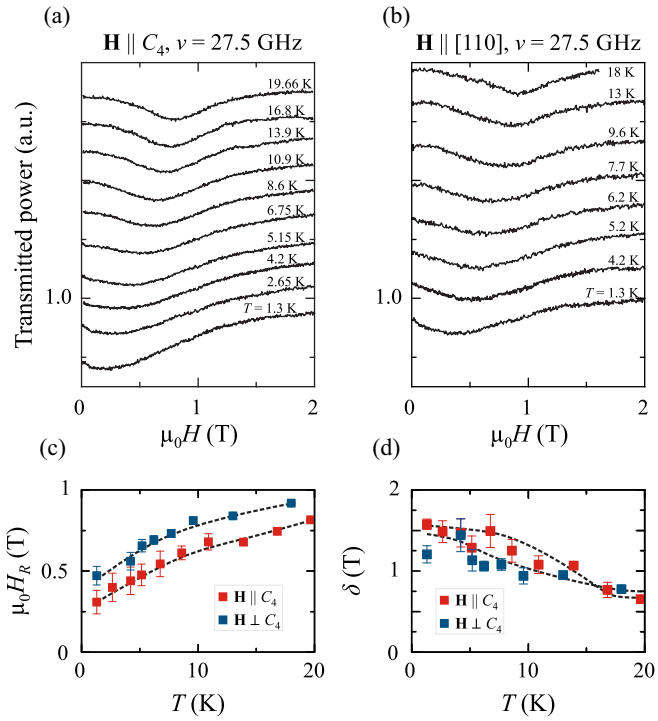

FIG. 8. (a) Temperature evolution of field scans $P_{tr}(H)$ at **H** || C_4, $\nu = 27.53$ GHz. (b) Temperature evolution of field scans $P_{tr}(H)$ at **H** || [110], $\nu = 27.53$ GHz. The scans were normalized to 1 and stacked along ordinate axis for clarity. (c) Temperature dependencies of resonance fields H_R. (d) Temperature dependencies of linewidths δ. Dashed lines in (c) and (d) are given as guides for eye.

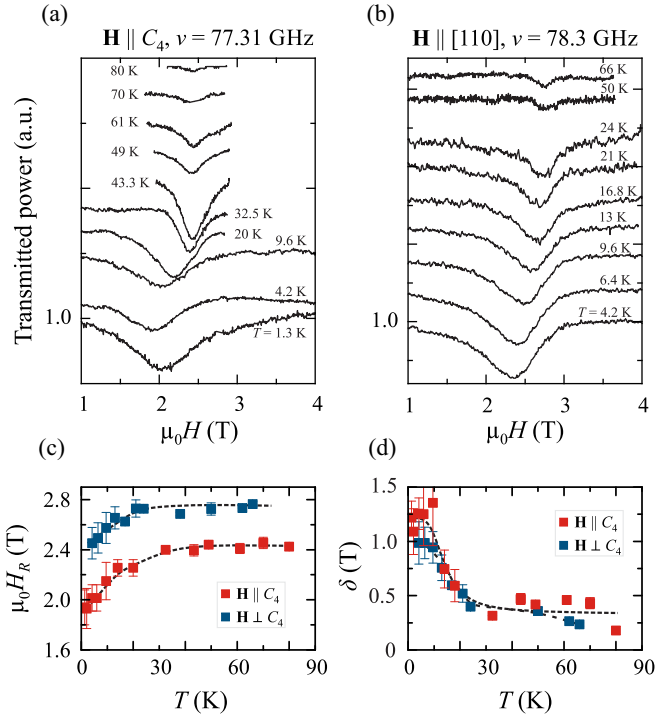

FIG. 9. (a) Temperature evolution of field scans $P_{tr}(H)$ at **H** || C_4, $\nu = 77.31$ GHz. (b) Temperature evolution of field scans $P_{tr}(H)$ at **H** || [110], $\nu = 78.3$ GHz. The scans were normalized to 1 and stacked along ordinate axis for clarity. (c) Temperature dependencies of resonance fields H_R. (d) Temperature dependences of linewidths δ. Dashed lines in (c) and (d) are given as guides for eye.

clarity. It can be seen that the intensity of resonance absorption decreases with increasing temperature as it does in a paramagnet. At low temperatures the lines are wide and shifted to low fields. As the temperature increases, the linewidth δ decreases and the resonance line shifts to the EPR field, which can be explained by the temperature decrease of the gap Δ. The values of $H_R(T)$ and $\delta(T)$ are shown in panels (c) and (d) of the corresponding figures, respectively. Error bars show the error of the obtained parameters. Errors for points without bars were less than the size of the symbol. It can be seen that at $T > 30$ K the absorption lines become paramagnetic. The gyromagnetic ratios derived from high-frequency measurements are: $\gamma_{\parallel} = 32 \pm 1$ GHz/T and $\gamma_{\perp} = 28 \pm 1$ GHz/T, which is in agreement with EPR measurements at $\nu = 9.35$ GHz.

Angular dependencies of H_R obtained at $T = 4.2$ K for **H** rotated in crystallographic planes (100) and (001) are shown in top and bottom panels of Fig. 10, respectively. α is the angle between **H** and [110] axis. The segments given at some points illustrate the characteristic values of the width at the half-maximum (HWHM) of the corresponding absorption lines. The solid line in top panel of Fig. 10 shows the approximation of the angular dependence with empirical harmonic dependence $\delta H \cos(2\alpha) + H_0$. The ratio of the maximal and minimal values of resonance field H_R at $T = 4.2$ K is $H_{R\max}/H_{R\min} = 1.3$, while at $T > 30$ K the ratio $H_{R\max}/H_{R\min} = 1.1$ agrees with the ratio obtained at $\nu = 9.35$ GHz. Anisotropy of H_R was not observed at rotation of magnetic field within the (001) plane.

In conclusion of this section, we summarize the results obtained with different experimental techniques in present work and in Refs. [19,20].

At $T = T_{c1}$, $LiCu_3O_3$ acquires magnetic order with wave vector $\mathbf{k} = (1/2, 0, 1/2)$ [20]. At the same time, according to the magnetometry measurements and EPR data, more than half of the magnetic ions resides in disordered state, and down to $T = 30$ K paramagnetic spectra are observed. At further temperature decrease, the excitation branch acquires a gap and becomes quasilinear. The value of the gap Δ monotonously increases as the temperature decreases. At $T = 4.2$ K the value of $\Delta = 25 \pm 3$ GHz. At the same time, in the whole experimental range, the deflection of the absorption line centers from the paramagnetic position $H_{pm} = \nu/\gamma$ does not exceed the halfwidth of lines. The quasilinear branch was observed at all orientations of the external magnetic field **H**. The observed anisotropy of the resonance field H_R can be reasonably explained by the anisotropy of gyromagnetic ratio γ. The studied branch is effectively excited by the magnetic component of UHF-radiation **h** oriented perpendicular to the external static magnetic field **H**. The transformation of ESR spectra at $T < 30$ K is accompanied by the significant broadening of the ^{7}Li NMR spectra [19] which indicates a rearrangement of the magnetic state of $LiCu_3O_3$ at this temperature range.

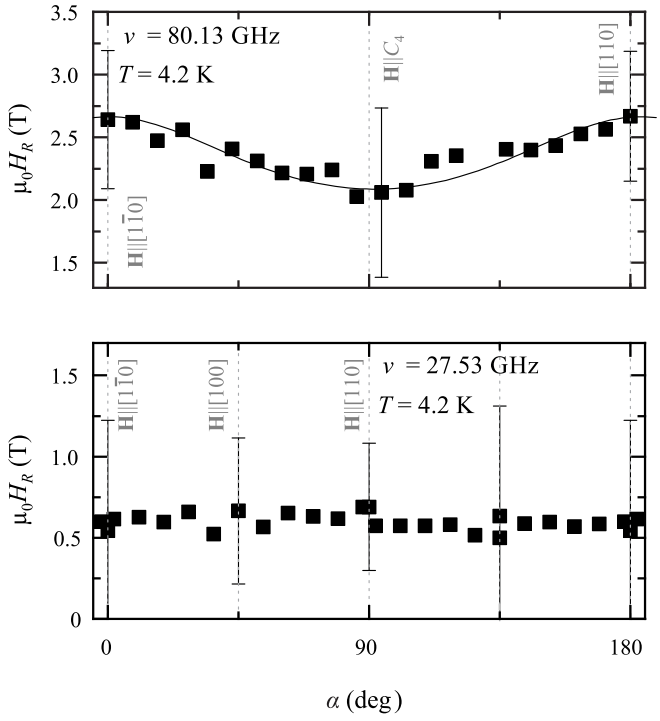

FIG. 10. (Top) Angular dependence of H_R at $T = 4.2$ K, $\nu = 80.13$ GHz. Magnetic field **H** was rotated from [110] axis to C_4 axis of the crystal. The solid line shows the approximation of the angular dependence with the empirical harmonic dependence. (Bottom) Angular dependence of H_R at $T = 4.2$ K, $\nu = 27.53$ GHz. Magnetic field **H** was rotated from [110] axis to [100] axis of the crystal. α is the angle between **H** and [1$\bar{1}$0] axis.

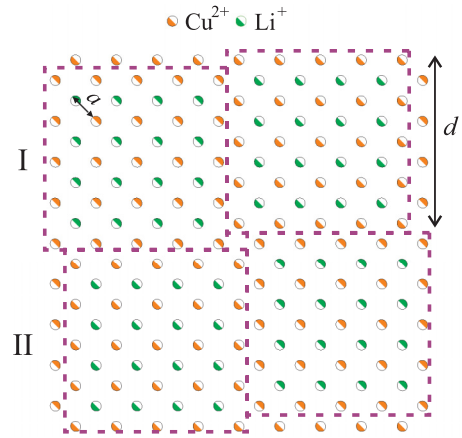

FIG. 11. Simplest model of domain structure of $LiCu_3O_3$ with square chessboard-ordered domains with $Li_{0.5}Cu_{0.5}O$ structure. Purple dashed lines mark domain boundaries. Half-shaded orange and green circles represent Cu^{2+} and Li^+ ions from different domains. Oxygen ions are omitted for clarity.

VI. DISCUSSION

In this section, we discuss the results within the model proposed in Ref. [19] which assumes the quasi-two-dimensionality of $LiCu_3O_3$ due to the layered crystal structure and the frustration of interplanar exchange interactions. It is suggested that at temperatures $T < T_{c1} \approx 123$ K, a collinear antiferromagnetic order is established in the crystallographic A planes where the ratio of magnetic Cu^{2+} ions is equal to 80% which essentially exceeds the percolation threshold for square lattice ($p_c \approx 0.59$). It is natural to expect the observation of the branches of antiferromagnetic resonance. Nevertheless, we did not detect any resonance features which could be ascribed to low-frequency oscillations of a collinear magnetic structure. Probably, the value of the corresponding ESR gap is above the studied frequency range. It is also possible that the linewidth of these resonance features does not allow their observation.

Below T_{c1}, a part of the crystal is not ordered and remains in paramagnetic state, which is evident because of the temperature dependence of the EPR line intensity $I(T)$ measured at $\nu = 9.35$ GHz. $I(T)$ is well described by the Curie-Weiss law at $30 < T < 120$ K with the Curie-Weiss constant $\theta_B = 7.5 \pm 1.5$ K [Figs. 4(c)–4(e)]. Note that the interpretation of the temperature dependence of the magnetic susceptibility $\chi(T)$ measured at $\mu_0 H = 0.3$ T is more complicated because both nonordered and antiferromagnetically ordered parts of the sample contribute in it. Assuming that the antiferromagnetic contribution is almost temperature-independent, the temperature derivative of $\chi(T)$ is determined solely by the paramagnetic part of the sample. The square-root of this derivative, $\sqrt{-d\chi(T)/dT}$, demonstrates a usual Curie-Weiss-law behavior. The Curie-Weiss constant obtained from linear approximation of $\sqrt{-d\chi(T)/dT}^{-1}$ is $\theta = 13 \pm 2$ K. This rough estimation is close to the value of θ_B obtained from the ESR experiments.

The average number of bonds per magnetic ion within the B planes can be estimated as 2.4 in assumption that Li^+ and Cu^{2+} ions are distributed randomly in ratio 0.4:0.6. Using the estimated number of bonds and the value of θ_B obtained from the ESR experiments, we evaluate the value of in-plane diagonal exchange integral as $J \approx 11.5 \pm 2.5$ K. At temperature $T < 30$ K, the ESR spectra acquires a gap Δ. The value of Δ gradually increases with temperature decrease up to $\Delta = 25 \pm 3$ GHz at $T = 4.2$ K. Initially, we associated this branch with the occurrence of magnetic order in B planes, but this hypothesis had to be rejected for the following reasons: (i) the gap occurrence has a gradual and monotonous type in contrast to traditional behavior at the transition from paramagnetic to ordered state; (ii) no additional branches of magnetic resonance one could expect to observe in collinear or planar structures were observed; (iii) the angular dependence of the quasilinear branch $\nu(H)$ can be qualitatively explained by the anisotropy of the g factor; and (iv) the temperature dependence of the intensity of the magnetic Bragg peak (1/2, 0, 1/2) obtained in elastic neutron scattering studies [20] does not demonstrate any additional peculiarities at $T_{c2} \approx 30$ K which could be expected in case that magnetic order in B planes occurred.

Thus, as the main hypothesis, we suppose that the observed gap in the magnetic resonance spectra is, in fact, a pseudogap of exchange nature defined by nonuniform distribution of magnetic ions in the B planes.

The dynamic properties of a two-dimensional Heisenberg antiferromagnet with $S = 1/2$ on a diluted square lattice have been theoretically studied in Ref. [10]. It has been shown that

for a square lattice with a dilution ratio x, spin-wave excitations in the range of the wavelengths $\lambda > l_0 = ae^{\frac{\pi}{4x}}$ are absent, and the excitation spectra are incoherent; here, a denotes the lattice constant. In the vicinity of ω_0, an anomalous density of magnetic excitations is expected. Qualitatively, the occurrence of localized excitations can be understood as the standing magnons in domains with effective size l_0. The characteristic frequency of localized excitations, according to Ref. [10], is $\omega_0 \sim c_0/l_0$, where $c_0 = 2\sqrt{2}SJa$ is the spin-wave velocity in a square lattice without dilution. In case of $LiCu_3O_3$, the characteristic cluster length for B planes ($x = 0.4$) is $l_0 \approx 7a$. Using the previously obtained estimation of the exchange integral $J = 11.5 \pm 2.5$ K, we obtain the estimation of the localized mode frequency $\omega_0 = 50 \pm 10$ GHz. The gap of ESR spectra obtained in low-temperature experiments is $\Delta = 25 \pm 3$ GHz, which is approximately 2 times smaller than ω_0. Such discrepancy might be due to the undervaluation of the characteristic size used in our estimations.

Note that these estimations were performed in frames of the model proposed in Ref. [10] in which nonmagnetic ions are distributed randomly. At the same time, as it was discussed in Sec. II, more energetically favorable situation is when $Li_{0.5}Cu_{0.5}O$ domains are formed. According to the Goodenough-Kanamori-Anderson rule, indirect exchange interaction between Cu^{2+} ions from neighboring domains can be expected to be much smaller than between copper ions inside the domains due to the 90° angle formed by copper ions from domains I and II and the interconnecting oxygen ion [see Fig. 2(d)]. This fact can explain quasiparamagnetic behavior of $LiCu_3O_3$ at $T << J$ in the frames of the suggested model. The characteristic size of the domains in this model sufficiently depends on geometry and determines the value of the pseudogap. Note that the pseudogap can be observed only at low temperatures when the correlation length exceeds the size of the clusters, which qualitatively explains the observed temperature dependence of ESR resonance field. The temperature dependence of the correlation length in the case of a square lattice is discussed, for instance, in Ref. [21].

The simplest model of chess-board ordered domains separated with domain borders on a square lattice presented in Fig. 11 gives the size of the clusters $d = \sqrt{2}a/(1-2x)$; for the B planes ($x = 0.4$), the characteristic size of domains is close to $7a$ obtained for the model of randomly distributed ions. In real samples of $LiCu_3O_3$, the surplus of Cu^{2+} in relation to 0.5 can be distributed randomly both inside the domain walls and the domains. In this case, the size of domains can be bigger than the estimation obtained before, which leads to the decrease of the expected value of the pseudogap. That is why our estimation can be considered as satisfying. Such pseudogap caused by nonmagnetic substitution was previously observed in quasi-one-dimensional magnets [5,6].

Finally, we would like to comment on the linewidth anisotropy of EPR line at intermediate temperature range 30 K $< T < T_{c1}$ (Fig. 5). The absolute value of the linewidth of $LiCu_3O_3$ is comparable to that of $LiCuVO_4$ [22]. In that compound the ring exchange via edge sharing Cu-O-Cu bridges was decisive for the explanation of the observed linewidth. The same situation occurs at the domain boundaries in $LiCu_3O_3$. Indeed, the majority of Cu^{2+} ions of each domain (16 from 25) contributes to the domain walls, if we assume the $Li_{0.5}Cu_{0.5}O_2$ ordered model as realistic, the 90° ring-exchange at the domain boundaries dominates the spin relaxation. In the

TABLE I. Crystal data and structure refinement for $LiCu_3O_3$.

Chemical formula	$Cu_{2.96}Li_{1.06}O_3$
Formula weight	242.37
Temperature, K	293
Crystal size, mm^3	$0.16 \times 0.11 \times 0.04$
System, space group, Z	tetragonal, $P4/mmm$, 1
a, Å	2.81386(2)
c, Å	8.89950(8)
Volume, $Å^3$	70.464(1)
ρ_{calc}, g/cm^3	5.712
μ, mm^{-1}	21.755
Radiation	Mo K_α ($\lambda = 0.71073$ Å)
Absorption correction	Analytical numeric absorption correction a multifaceted crystal model based on expressions [23]
T_{min}/T_{max}	0.116/0.460
Index ranges h, k, l	$-7 \leqslant h \leqslant 6, -7 \leqslant k \leqslant 7, -22 \leqslant l \leqslant 22$
θ°_{max}	65.1
Number of measured reflections/ number of independent reflections/ number of reflections with $I \geqslant 2\sigma\ (I)$	21485/438/436
Data/restraints/parameters	438/4/18
Extinction coefficient	0.39(2)
R_{int}, R_σ	0.039/0.0073
$R[F^2 > 2\sigma(F^2)]/wR(F^2)$	0.017/0.048
Goodness-of-fit on F^2	1.168
Largest diff. peak/hole, $e/Å^{-3}$	1.45/−2.14

TABLE II. Fractional atomic coordinates, isotropic or equivalent isotropic displacement parameters U^*_{iso}/U_{eq} (Å^2) and atomic occupancy for $LiCu_3O_3$.

Atom	Site	x/a	y/b	z/c	U^*_{iso}/U_{eq}	Occ. (<1)
Cu(1)	1a	0.000000	0.000000	0.000000	0.00960 (4)	
Cu(2)	1b	0.000000	0.000000	0.500000	0.00625 (5)	0.810 (2)
Li(2)	1b	0.000000	0.000000	0.500000	0.00625 (5)	0.185 (9)
Cu(3)	2h	0.500000	0.500000	0.22744 (3)	0.00701 (5)	0.5761 (18)
Li(3)	2h	0.500000	0.500000	0.22744 (3)	0.00701 (5)	0.435 (9)
O(1)	1d	0.500000	0.500000	0.500000	0.00958 (14)	
O(2)	2g	0.000000	0.000000	0.21008 (10)	0.00871 (10)	

ideal case, the ratio of $\Delta H_\parallel$ to $\Delta H_\perp$ should be 2:1. However, inevitable ionic Li^+/Cu^{2+} disorder and contributions from the inner Cu^{2+} ions of the domains are expected to reduce this ideal ratio. Hence, the observed ratio 1.6:1.4 still supports the basic relaxation via symmetric anisotropic exchange in the Cu-O-Cu bridges.

VII. CONCLUSION

In this work, we conducted an experimental study of the magnetic structure of $LiCu_3O_3$ by means of electron spin resonance. According to the results of x-ray structure study, the crystallographic structure of $LiCu_3O_3$ consists of alternating square lattice layers with compositions $Li_{0.2}Cu_{0.8}O$ (A planes) and $Li_{0.4}Cu_{0.6}O$ (B planes). Lattice parameters and dilution ratios are close to those obtained for samples grown in other experimental groups [17,20]. The results of the ESR experiments can be explained in assumption that the magnetic ions from planes with higher concentration of magnetic ions order antiferromagnetically at $T = 123$ K, while magnetic ions from more depleted planes remain in paramagnetic state. The observed quasiparamagnetic branch in the ESR spectra at $T < 30$ K can be interpreted as magnetic resonance in the disordered B planes. Estimations of the values of the pseudogap conducted in frames of the model of randomly distributed ions and in frames of the model of domain formation in B planes are close to the value observed experimentally.

ACKNOWLEDGMENTS

We are grateful to A. B. Drovosekov, E. G. Nikolaev, A. I. Smirnov, and S. S. Sosin for fruitful discussions. The work was financially supported by Russian Science Foundation, Grant No 22-12-00259 (ESR measurements and data analysis) and the Basic Research Program of HSE (EPR data analysis). This work was partially supported by the Deutsche Forschungsgemeinschaft (DFG) within the Transregional Collaborative Research Center TRR 360 "Constrained Quantum Matter," Project No. 492547816 (Augsburg, Munich, Stuttgart, Leipzig). M.H. and H.-A.K.v.N. acknowledge funding within the joint RFBR–DFG research project, Contracts No. 19-51-45001 and No. KR2254/3-1. Part of the work (on single crystals growth) performed at the RTU MIREA was funded by the Ministry of Science and Higher Education of the Russian Federation within the framework of the State Task (FSFZ-2023-0005 project). X-ray diffraction analysis was carried out within the state assignment of NRC "Kurchatov Institute" using the equipment of the Shared Research Center of Kurchatov Complex Crystallography and Photonics of NRC "Kurchatov Institute."

APPENDIX: SINGLE-CRYSTAL X-RAY DIFFRACTION STUDY OF $LiCu_3O_3$

X-ray diffraction data were collected at room temperature by means of the Xcalibur EosS2 single crystal x-ray diffractometer operating with monochromatic MoKα radiation. The intensities of reflections were processed and numerically corrected for absorption effects based on Gaussian integration over a multifaceted crystal model [23] implemented in SCALE3 ABSPACK scaling algorithm using the CRYSALIS PRO 171.43.122a program [24]. All calculations in the crystal structure solution and refinement were performed within the OLEX2 software package [25]. The atomic positions were located using direct methods and refined using a combination of Fourier synthesis and least-squares refinement in anisotropic approximations using SHELX software [26,27]. In the first step, the crystal structure was refined with all three cationic positions completely occupied by Cu atoms. The refinement of this model was completed with a high R factor of 16% and large residual peak values on the electron density difference maps. The successive refinement of

TABLE III. Selected bond lengths (Å) for $LiCu_3O_3$. Symmetry codes: (i) $x, y+1, z$; (ii) $x, y-1, z$; (iii) $x+1, y, z$; (iv) $x-1, y, z$; (v) $-x, -y, -z$; (vi) $-x, -y+1, -z$; (vii) $x-1, y-1, z$; (viii) $x+1, y+1, z$; (ix) $-x+1, -y+1, -z+1$.

Cu(1)—Cu(1)^i	2.8139 (1)	Cu(2)—Cu(2)^i	2.8139 (1)
Cu(1)—Cu(1)^{ii}	2.8139 (1)	Cu(2)—O(1)^{vii}	1.9897 (1)
Cu(1)—Cu(1)^{iii}	2.8139 (1)	Cu(2)—O(1)	1.9897 (1)
Cu(1)—Cu(1)^{iv}	2.8139 (1)	Cu(2)—O(1)^{ii}	1.9897 (1)
Cu(1)—Cu(3)	2.8383 (2)	Cu(2)—O(1)^{iv}	1.9897 (1)
Cu(1)—Cu(3)^{iv}	2.8383 (2)	Cu(3)—Cu(3)^{ii}	2.8139 (1)
Cu(1)—Cu(3)^{ii}	2.8383 (2)	Cu(3)—Cu(3)^{iii}	2.8139 (1)
Cu(1)—Cu(3)^{v}	2.8383 (2)	Cu(3)—Cu(3)^{iv}	2.8139 (1)
Cu(1)—Cu(3)^{vi}	2.8383 (2)	Cu(3)—Cu(3)^{i}	2.8139 (1)
Cu(1)—O(2)	1.8696 (9)	Cu(3)—O(1)	2.4256 (3)
Cu(1)—O(2)^{v}	1.8696 (9)	Cu(3)—O(2)	1.9957 (1)
Cu(2)—Cu(2)^{ii}	2.8139 (1)	Cu(3)—O(2)^{i}	1.9957 (1)
Cu(2)—Cu(2)^{iv}	2.8139 (1)	Cu(3)—O(2)^{iii}	1.9957 (1)
Cu(2)—Cu(2)^{iii}	2.8139 (1)	Cu(3)—O(2)^{viii}	1.9957 (1)

the occupancies for the mixed atomic positions Cu(3) with initial values of 60%Cu + 40%Li and Cu(2) with initial values of 80%Cu + 20%Li and the refinement of the extinction parameter converged to the R factor of 1.7%. The final refined composition of mixed atomic positions 81%Cu(2) + 18.5%Li(2), 57.6%Cu(3) + 43.5%Li(3) gave the resulting formula $Cu_{2.96}Li_{1.06}O_3$. The crystallographic parameters, experimental conditions of the data collection, and the structural refinement results are summarized in Table I. Atomic positions, displacement parameters and occupancies are given in Table II. Selected interatomic distances are given in Table III. CSD 2402337 contains the supplementary crystallographic data for this paper. These data can be obtained free of charge from FIZ Karlsruhe, see Ref. [28].

[1] I. Ya. Korenblit and E. F. Shender, Diluted quasi-one-dimensional classical antiferromagnets, Phys. Rev. B **48**, 9478 (1993).

[2] C. Dupas and J.-P. Renard, Effect of impurities on the Néel temperature and the low-temperature magnetic susceptibility of the quasi-one-dimensional antiferromagnet TMMC, Phys. Rev. B **18**, 401 (1978).

[3] J. C. Shouten, K. Kopinga, and W. J. M. de Jonge, The susceptibility of DMMC;Cd: A diluted 1D anisotropic Heisenberg system, J. Phys. C: Solid State Phys. **15**, 783 (1982).

[4] I. Yamada and Y. Natsume, Dynamic effect of low-symmetric distribution of spins on EPR lines in one-dimensional magnetic systems. II. Enhancement by Cu doping in TMMC, J. Phys. Soc. Jpn. **48**, 58 (1980).

[5] G. Simutis, S. Gvasaliya, M. Månsson, A. L. Chernyshev, A. Mohan, S. Singh, C. Hess, A. T. Savici, A. I. Kolesnikov, A. Piovano, T. Perring, I. Zaliznyak, B. Büchner, and A. Zheludev, Spin Pseudogap in Ni-Doped $SrCuO_2$, Phys. Rev. Lett. **111**, 067204 (2013).

[6] G. Simutis, S. Gvasaliya, N. S. Beesetty, T. Yoshida, J. Robert, S. Petit, A. I. Kolesnikov, M. B. Stone, F. Bourdarot, H. C. Walker, D. T. Adroja, O. Sobolev, C. Hess, T. Masuda, A. Revcolevschi, B. Büchner, and A. Zheludev, Spin pseudogap in the $S = 1/2$ chain material Sr_2CuO_3 with impurities, Phys. Rev. B **95**, 054409 (2017).

[7] S. S. Sosin, I. A. Zaliznyak, L. A. Prozorova, Yu. M. Tsipenyuk, and S. V. Petrov, Influence of a nonmagnetic impurity on the properties of the quasi-one-dimensional antiferromagnet $CsNiCl_3$, J. Exp. Theor. Phys. **85**, 114 (1997).

[8] K. Kato, S. Todo, K. Harada, N. Kawashima, S. Miyashita, and H. Takayama, Quantum phase transition of the randomly diluted Heisenberg antiferromagnet on a square lattice, Phys. Rev. Lett. **84**, 4204 (2000).

[9] A. W. Sandvik, Classical percolation transition in the diluted two-dimensional $S = 1/2$ Heisenberg antiferromagnet, Phys. Rev. B **66**, 024418 (2002).

[10] A. L. Chernyshev, Y. C. Chen, and A. H. Castro Neto, Diluted quantum antiferromagnets: Spin excitations and long-range order, Phys. Rev. B **65**, 104407 (2002).

[11] P. Carretta, G. Prando, S. Sanna, R. De Renzi, C. Decorse, and P. Berthet, Evidence for impurity-induced frustration in La_2CuO_4, Phys. Rev. B **83**, 180411(R) (2011).

[12] O. P. Vajk, P. K. Mang, M. Greven, P. M. Gehring, and J. W. Lynn, Quantum impurities in the two-dimensional spin one-half Heisenberg antiferromagnet, Science **295**, 1691 (2002).

[13] N. Papinutto, P. Carretta, S. Gonthier, and P. Millet, Spin dilution in frustrated two-dimensional $S = 1/2$ antiferromagnets on a square lattice, Phys. Rev. B **71**, 174425 (2005).

[14] Y. Endoh, K. Yamada, R. J. Birgeneau, D. R. Gabbe, H. P. Jenssen, M. A. Kastner, C. J. Peters, P. J. Picone, T. R. Thurston, J. M. Tranquada, G. Shirane, Y. Hidaka, M. Oda, Y. Enomoto, M. Suzuki, and T. Murakami, Static and dynamic spin correlations in pure and doped La_2CuO_4, Phys. Rev. B **37**, 7443 (1988).

[15] S. J. Hibble, J. Kohler, A. Simon, and S. Paider, $LiCu_2O_2$ and $LiCu_3O_3$: New mixed valent copper oxides, J. Solid State Chem. **88**, 534 (1990).

[16] R. Berger, P. Önnerud, and R. Tellgren, Structure refinements of $LiCu_2O_2$ and $LiCu_3O_3$ from neutron powder diffraction data, J. Alloys Compd. **184**, 315 (1992).

[17] A. A. Bush, K. E. Kamentsev, and E. A. Tishchenko, Growth and properties of $LiCu_2O_2$-$NaCu_2O_2$ crystals, Inorg. Mater. **55**, 374 (2019).

[18] See Supplemental Material in Ref. [20].

[19] A. A. Bush, S. K. Gotovko, V. Yu. Ivanov, V. I. Kozlov, E. G. Nikolaev, and L. E. Svistov, Magnetic properties of $LiCu_3O_3$: A quasi-two-dimensional antiferromagnet on a depleted square lattice, Phys. Rev. B **109**, 115151 (2024).

[20] A. Consiglio, G. Gatti, E. Martino, L. Moreschini, J. C. Johannsen, K. Prša, P. G. Freeman, D. Sheptyakov, H. M. Rønnow, R. Scopelliti, A. Magrez, L. Forró, C. Schmitt, V. Jovic, C. Jozwiak, A. Bostwick, E. Rotenberg, T. Hofmann, R. Thomale, G. Sangiovanni *et al.*, Electron glass phase with resilient Zhang-Rice singlets in $LiCu_3O_3$, Phys. Rev. Lett. **132**, 126502 (2024).

[21] R. J. Birgeneau, M. Greven, M. A. Kastner, Y. S. Lee, B. O. Wells, Y. Endoh, K. Yamada, and G. Shirane, Instantenious spin correlations in La_2CuO_4, Phys. Rev. B **59**, 13788 (1999).

[22] H.-A. Krug von Nidda, L. E. Svistov, M. V. Eremin, R. M. Eremina, A. Loidl, V. Kataev, A. Validov, A. Prokofiev, and W. Aßmus, Anisotropic exchange in $LiCuVO_4$ probed by ESR, Phys. Rev. B **65**, 134445 (2002).

[23] R. C. Clark and J. S. Reid, The analytical calculation of absorption in multifaceted crystals, Acta Crystallogr. A: Found. Crystallogr. **51**, 887 (1995).

[24] Rigaku Oxford Diffraction, *CrysAlisPro Software system, version 1.171.42.62* (Rigaku Corporation, Wroclaw, Poland, 2022).

[25] O. V. Dolomanov, L. J. Bourhis, R. J. Gildea, J. A. K. Howard, and H. Puschmann, *OLEX2:* A complete structure solution, refinement and analysis program, J. Appl. Crystallogr. **42**, 339 (2009).

[26] G. M. Sheldrick, A short history of SHELX, Acta Crystallogr. A: Found. Crystallogr. **64**, 112 (2008).

[27] G. M. Sheldrick, Crystal structure refinement with SHELXL, Acta Crystallogr. C: Struct. Chem. **71**, 3 (2015).

[28] https://www.ccdc.cam.ac.uk/structures.